

## Comparison of microporous MFI and dense Pd membrane performances in an extractor-type CMR

L. van Dyk<sup>a</sup>, S. Miachon<sup>b</sup>, L. Lorenzen<sup>a</sup>, M. Torres<sup>c</sup>, K. Fiaty<sup>d</sup>, J.-A. Dalmon<sup>b,\*</sup>

<sup>a</sup> University of Stellenbosch, Matieland, 7602 Stellenbosch, South Africa

<sup>b</sup> IRC-CNRS-Lyon, 2 av. Albert Einstein, 69626 Villeurbanne Cedex, France

<sup>c</sup> Universidad Autonoma Metropolitana (Azcapotzalco), San Pablo sn, Mexico

<sup>d</sup> LAGEP, UCB-CPE Lyon, 43 bd. du 11 Nov. 1918, 69622 Villeurbanne Cedex, France

### Abstract

An extractor-type CMR, including a Pt-based fixed-bed catalyst, was combined with two different membranes, either a Pd membrane, obtained by electroless plating, or an MFI zeolite membrane, obtained by hydrothermal synthesis. These two configurations were compared in isobutane dehydrogenation. Both CMRs give better results than conventional reactors. However, though the two membranes presented different separative properties, the two CMRs showed very similar yields. This has been attributed to the limitation of both CMRs by the catalyst lack of efficiency, when compared to the membrane performance. A modeling approach that combines catalyst kinetic law and membrane gas transfer equations also contributes to the description of the CMRs performance.

© 2003 Elsevier B.V. All rights reserved.

*Keywords:* Pd membrane; MFI membrane; Extractor-type CMR; Isobutane dehydrogenation

### 1. Introduction

According to a recently proposed classification of CMRs [1], in an extractor, the role of the membrane is to selectively remove (extract) from the reactor a product of the reaction. When compared to conventional reactors, this may lead either to an improved yield in the case of equilibrium-restricted reactions, like hydrocarbon dehydrogenation [2], or to an improved selectivity in consecutive reactions when the permeation favors the extraction of a primary product [3].

Here we report on the performances of a Pd membrane or an MFI membrane, used as hydrogen extracting membranes during the isobutane dehydrogenation.

If this reaction has been already studied in CMRs using either dense Pd [4–6] or porous materials [7–9], no comparative experimental data under similar conditions have been reported. The dehydrogenation of isobutane to isobutene is the first step in the production of MTBE, an octane booster for gasoline. Though recent regulation about oxygenates in motor fuels leads to reconsider the isobutene demand in the future, the isobutane dehydrogenation can be considered as a good model reaction for membrane reactors of the extractor type [9].

Identical reaction conditions were used in order to compare the performances of these two membranes that possess very different characteristics and properties. In principle, Pd membranes are perfectly selective for hydrogen, as permeation is due to the formation of palladium hydrides. However, they are expensive and may present stability problems [10].

\* Corresponding author. Tel.: +33-4-7244-5368;

fax: +34-7244-5399.

E-mail address: dalmon@catalyse.univ-lyon1.fr (J.-A. Dalmon).

**Nomenclature**

$D_i^m$	diffusion coefficient of species $i$ through the membrane ( $\text{mm}^2 \text{min}^{-1}$ )
$D_i^s$	molecular diffusivity of species $i$ ( $\text{mm}^2 \text{min}^{-1}$ )
$F_i^{(k)}$	molar flow rate of species $i$ in zone $k$ ( $\text{mol min}^{-1}$ )
$F_{i,0}^{(k)}$	inlet molar flow rate of species $i$ in zone $k$ ( $\text{mol min}^{-1}$ )
$F_T^{(k)}$	total molar flow rate in zone $k$ ( $\text{mol min}^{-1}$ )
$k_1$	kinetic constant for reaction ( $\text{mol min}^{-1} \text{g}^{-1}$ )
$K_{\text{eq}}$	equilibrium constant ( $\text{atm}^{-1}$ )
$K_{iC_4}$	adsorption equilibrium constant of isobutane ( $\text{atm}^{-1}$ )
$K_{iC_4=}$	adsorption equilibrium constant of isobutene ( $\text{atm}^{-1}$ )
$K_{H_2}$	adsorption equilibrium constant of hydrogen ( $\text{atm}^{-1}$ )
$L$	reactor length (mm)
$P$	Total pressure in the catalyst bed and in the shell side (atm)
$P_{H_2}$	partial pressure of hydrogen (atm)
$P_{iC_4}$	partial pressure of isobutane (atm)
$P_{iC_4=}$	partial pressure of isobutene (atm)
$Q$	reaction quotient ( $\text{atm}^{-1}$ )
$r$	rate of reaction ( $\text{mol min}^{-1} \text{g}^{-1}$ )
$r$	radial coordinate (in <a href="#">Appendix A</a> )
$R$	gas law constant
$R_0$	radius of the thermometric tube (mm)
$R_1$	inner radius of the membrane tube (mm)
$R_2$	outer radius of the membrane tube (mm)
$R_3$	inner radius of the shell tube (mm)
$R_4$	outer radius of the shell tube (mm)
$S_f$	separation factor
$T$	reaction temperature (K)
$z$	axial coordinate

**Greek letters**

$\varepsilon_m, \varepsilon_s$	porosity of membrane, support
$\eta$	effectiveness factor

$\nu_i$	algebraic stoichiometry coefficient of specie $i$
$\rho$	catalyst apparent density ( $\text{g mm}^{-3}$ )
$\tau_m, \tau_s$	tortuosity of membrane, support

On the other hand, transport through zeolite membranes is very often controlled by diffusivity parameters and adsorption properties. Their selectivity may be strongly temperature-dependent.

Finally, the catalyst itself, here located as fixed-bed in the lumen of the tubular membrane, may operate under conditions that are quite different from that of a conventional reactor. A modeling approach has been developed in order to illustrate how the CMR works.

**2. Experimental****2.1. Materials****2.1.1. Catalyst**

The *catalyst* was a trimetallic Pt–In–Ge supported on an MFI zeolite [11]. Indium and germanium were introduced within the zeolite precursors before hydrothermal synthesis. After calcination the final material contained 0.8 wt.% of both indium and germanium. Platinum (0.5 wt.%) was then introduced in the zeolite via an exchange/impregnation technique using  $\text{Pt}(\text{NH}_3)_4(\text{OH})_2$  as a precursor. Before catalytic use, the solid was activated in situ under flowing  $\text{H}_2$  at 823 K during 10 h. For experiments in the membrane reactor, and in order to avoid an excessive pressure drop in the catalyst bed, the catalyst powder was transformed into pellets of ca. 2 mm size, using a lab extruder.

**2.1.2. Membranes**

The separative phases (Pd or MFI) were applied on ceramic tubular supports (Pall-Exekia T1-70), consisting of three macroporous  $\alpha$ -alumina layers (from outer to inner side, respective average pore sizes: 12, 0.8, 0.2  $\mu\text{m}$  and thicknesses 1500, 40, 20  $\mu\text{m}$ ).

**2.1.2.1. Pd membrane.** The palladium membrane was prepared by a batch electroless plating technique.

Table 1  
Composition of palladium (1625 ppm Pd) plating bath per liter of plating solution

(NH <sub>3</sub> ) <sub>4</sub> PdCl <sub>2</sub> ·H <sub>2</sub> O (g)	4.00
28 wt.% ammonia (ml)	325
EDTA (g)	65
35 wt.% hydrazine	Hydrazine: Pd=0.35:1 (start reaction), increased with time
Temperature (°C)	72

A detailed discussion description of the plating procedure and equipment is given in [12]. The pretreated support membrane was sealed in a Teflon reactor and placed in a warm bath (345 K), after which 8 ml of plating solution (Table 1) was introduced in the inner volume of the tubular support. Hydrazine was only added at the start of a plating session and increased with time (Table 2). An initial layer of 1 μm was plated without a vacuum being drawn and the membrane cleaned with 15 wt.% ammonia solution. For subsequent layers a vacuum was drawn on the membrane.

**2.1.2.2. Zeolite membrane.** The MFI membrane was obtained by synthesis of zeolite crystals inside the pores of the macroporous tubular support (pore-plugging method) [13]. The precursor solution of the MFI zeolite was obtained by mixing silica (Aerosil 380) and a template (tetrapropylammonium hydroxide, TPAOH). After a 3-day ageing period, that solution was poured in a Teflon-lined autoclave containing the porous ceramic tube. Hydrothermal synthesis was then performed at 443 K for 3 days, and the membrane was calcined at 773 K under a flow of 5% O<sub>2</sub> diluted in N<sub>2</sub>. Characterization of the membrane showed it could be considered defect-free

Table 2  
Plating procedure for producing Pd films

Reaction time (total) (8 ml plating solution) (min)	1.75 wt.% hydrazine added (8 ml plating solution) (μl)
0	84.8
20	56.5
40	283
Stop reaction after 60 min	

(i.e. the transport through the membrane is controlled by the micropores of the MFI structure).

## 2.2. Transport measurements: single gas and mixtures

The membranes were sealed with cylindrical graphite seals in a stainless steel module, equipped with temperature control. The lumen of the tubes was packed with inerts in order to simulate the catalysts pellets. Before membrane testing the palladium and MFI membranes were pretreated. The Pd membrane was pretreated at 593 K first in nitrogen then in oxygen; the same procedure was repeated at 723 K [12]. The MFI membrane was heated to 773 K in nitrogen and left for 4 h.

Single gas permeation measurements were performed for hydrogen, nitrogen and isobutane at 723 K in the dead-end mode. Separation tests on the MFI membrane were performed by a modified Wicke–Kallenbach method with a mixture of isobutane and hydrogen diluted in nitrogen, feed rate of 1.2 l/h (0.2 H<sub>2</sub>, 0.2 *i*C<sub>4</sub>H<sub>10</sub>, 0.6N<sub>2</sub>) with 1.2 l/h counter current nitrogen sweep. The separation factor (*S<sub>f</sub>*) was determined with the following formula:

$$S_f \left( \frac{H_2}{iC_4} \right) = \frac{([H_2]/[iC_4])_{\text{permeate}}}{([H_2]/[iC_4])_{\text{feed}}} \quad (1)$$

## 2.3. CMR operation and set-up

The fix-bed catalyst was packed in the lumen of the tubular membrane and the isobutane dehydrogenation reaction was carried out at 723 K and 50 ml/min feed flow (0.2 H<sub>2</sub>: 0.2 *i*C<sub>4</sub>H<sub>10</sub> and 0.6N<sub>2</sub>). The differential pressure across the membrane was kept at zero by varying the external pressure of the membrane module. Nitrogen was used as a sweep gas in the counter current mode at different flow rates. The feed and sweep flow rates were controlled with mass flow controllers (Brooks MFC). The compositions of the feed, permeate and retentate were analyzed on-line with a gas chromatograph (Shimadzu, GC 14A) equipped with two detectors: TCD for hydrogen and FID for hydrocarbons. The flow rates of the permeate and retentate were measured with an automatic flowmeter (Bios, Dry Cal DC-Lite).

### 3. Modeling

In order to interpret the results, the membrane reactor has been described through a theoretical model, combining transport equations and catalysis kinetics. A detailed model was previously presented by Casanave et al. [14]. Here, we will give a modified and more simple version, which is well-adapted for the purpose of this study.

Transport parameters were obtained from permeation measurements, as described in a previous section. The reaction rate expression employed is that obtained by Casanave et al. [15] on a similar catalyst, using a differential microreactor. When operating in the vicinity of thermodynamic equilibrium its expression is

$$r = \frac{k_1 K_{iC_4} (P_{iC_4} - P_{iC_4} = P_{H_2} / K_{eq})}{(1 + K_{iC_4} P_{iC_4} + K_{iC_4} = P_{iC_4} + \sqrt{K_{H_2} P_{H_2}})^2} \quad (2)$$

From this equation and the transport parameters, a one-dimensional model was developed using the following simplifying assumptions: operation in steady-state, isothermal conditions, negligible trans-membrane pressure, plug flow prevails in each compartment, axial dispersion negligible. Pressure drops through packed-bed and shell side are negligible. Gaseous components behave as ideal gases.

In order to take into account back permeation of the sweep gas, variations of the overall molar flow in the tube and shell sides are considered, owing to the chemical reaction and mass transfers through the porous media. Under the experimental conditions, Fick's law

is sufficient to describe mass transfers through the membrane. Only the simulation results of the counter-current configuration will be presented here.

Let us consider an element of length  $dz$  (see Fig. 1, schematic of the CMR). The differential equations describing mass balances in the axial direction for  $i = iC_4H_{10}$  (isobutane, also noted  $iC_4$ ),  $iC_4H_8$  (isobutene, also noted  $iC_4=$ ),  $H_2$  and  $N_2$  are (see Appendix A for details) can be obtained as follows.

#### 3.1. Tube side

For each component  $i$ , the evolution of the molar flow rate along the reactor length is

$$\begin{aligned} \frac{dF_i^{(1)}}{dz} = & v_i \eta \rho \pi (R_1^2 - R_0^2) r \\ & + 2\pi \frac{P}{RT} \frac{D_i^m \varepsilon_m}{\tau_m} \frac{1}{\ln(R_2/R_1) + (D_i^m \varepsilon_m / D_i^s \varepsilon_s) \times (\tau_s / \tau_m) \ln(R_3/R_2)} \\ & \times \left( \frac{F_i^{(2)}}{F_T^{(2)}} - \frac{F_i^{(1)}}{F_T^{(1)}} \right) \end{aligned} \quad (3)$$

The second term on the right-hand side of Eq. (3) renders the molar flow rate through the porous membrane. The apparent density  $\rho$  is defined as the mass of catalyst with respect to the tube unit volume,  $v_i$  is the algebraic stoichiometric coefficient of component  $i$ . The effectiveness factor,  $\eta$ , is introduced to account for some limiting effects on the activity of the catalyst in the CMR, when compared to that measured in the differential microreactor. Let us underline that  $\eta$  here has nothing to do with diffusion limitations in the catalyst. It is just an adjustment term that will be used

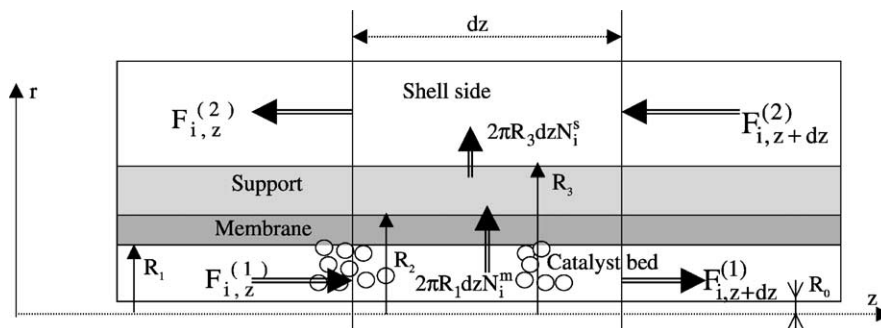


Fig. 1. Schematic view of the reactor in counter current mode. The reactor is divided into four zones: catalyst bed, membrane layer, and support and shell side.

to quantify differences between model data (kinetics and transmembrane transfers analyzed separately) and experimental results obtained in the CMR. The diffusivity coefficients  $D_i^m$  were estimated from permeation measurements with the membrane. Terms  $D_i^s$  are molecular diffusivities that were calculated from the kinetic theory of gases.

Adding Eq. (3) for each component of the gas stream and considering that the operation pressure is constant, the overall mass balance is

$$\frac{dF_T^{(1)}}{dz} = -2\pi \frac{P}{RT} \sum_{j \neq I} \frac{(D_I^m - D_j^m) \varepsilon_m}{\tau_m} \times \frac{1}{\ln(R_2/R_1) + (D_j^m \varepsilon_m / D_j^s \varepsilon_s) \times (\tau_s / \tau_m) \ln(R_3/R_2)} \times \left( \frac{F_j^{(2)}}{F_T^{(2)}} - \frac{F_j^{(1)}}{F_T^{(1)}} \right) + \eta \rho \pi (R_1^2 - R_0^2) r \Delta v \quad (4)$$

where  $\Delta v = \sum_i v_i$ .

### 3.2. Shell side material balance

For each component  $i \neq I$  ( $I$  being an inert or sweep gas)

$$\frac{dF_i^{(2)}}{dz} = (-1)^{n+1} 2\pi \frac{P}{RT} \frac{D_i^m \varepsilon_m}{\tau_m} \times \frac{1}{\ln(R_2/R_1) + (D_i^m \varepsilon_m / D_i^s \varepsilon_s) \times (\tau_s / \tau_m) \ln(R_3/R_2)} \times \left( \frac{F_i^{(2)}}{F_T^{(2)}} - \frac{F_i^{(1)}}{F_T^{(1)}} \right) \quad (5)$$

( $n = 1$  for counter current).

The overall mass balance in the shell side is

$$\frac{dF_T^{(2)}}{dz} = (-1)^n 2\pi \frac{P}{RT} \sum_{j \neq I} \frac{(D_I^m - D_j^m) \varepsilon_m}{\tau_m} \times \frac{1}{\ln(R_2/R_1) + (D_j^m \varepsilon_m / D_j^s \varepsilon_s) \times (\tau_s / \tau_m) \ln(R_3/R_2)} \times \left( \frac{F_j^{(2)}}{F_T^{(2)}} - \frac{F_j^{(1)}}{F_T^{(1)}} \right) \quad (6)$$

Table 3

Parameters used for simulation

$k_1 = 67 \mu\text{mol s}^{-1} \text{g}^{-1}$	$R_1 = 3.5 \text{ mm}$	$\varepsilon_s = 0.26$
$K_{iC_4} = 0.9 \text{ atm}^{-1}$	$R_2 = 3.505 \text{ mm}$	$\varepsilon_m = 0.5$
$K_{iC_4} = 2.1 \text{ atm}^{-1}$	$R_3 = 5 \text{ mm}$	$\tau_s = 1.5$
$K_{H_2} = 0.8 \text{ atm}^{-1}$	$R_4 = 8 \text{ mm}$	$\tau_m = 1$
$K_{eq} = 0.033$	$R_0 = 8 \text{ mm}$	
$\rho = 0.53 \text{ g cm}^{-3}$	$L = 100 \text{ mm}$	
Zeolite		Palladium
$D_{iC_4}^m = 6.1 \times 10^{-4} \text{ mm}^2 \text{ s}^{-1}$	$D_{iC_4}^m = 3 \times 10^{-3} \text{ mm}^2 \text{ s}^{-1}$	
$D_{iC_4}^m = 6.1 \times 10^{-4} \text{ mm}^2 \text{ s}^{-1}$	$D_{iC_4}^m = 3 \times 10^{-3} \text{ mm}^2 \text{ s}^{-1}$	
$D_{H_2}^m = 0.036 \text{ mm}^2 \text{ s}^{-1}$	$D_{H_2}^m = 0.09 \text{ mm}^2 \text{ s}^{-1}$	
$D_{N_2}^m = 0.012 \text{ mm}^2 \text{ s}^{-1}$	$D_{N_2}^m = 3 \times 10^{-3} \text{ mm}^2 \text{ s}^{-1}$	

The boundary conditions for Eqs. (3)–(6) are

- tube side (at  $z = 0$ )

$$F_i^{(1)} = F_{i,0}^{(1)} \quad (7)$$

$$F_T^{(1)} = \sum_i F_{i,0}^{(1)} \quad (8)$$

- shell side (at  $z = L$  (counter current))

$$F_i^{(2)} = F_{i,0}^{(2)} \quad (9)$$

$$F_T^{(2)} = \sum_i F_{i,0}^{(2)} \quad (10)$$

The system of differential equations (3)–(6) was rearranged by introducing dimensionless length.

Orthogonal collocation was applied for numerical discretization of the above-mentioned equations and IMSL routine DN2QNF was used for resolution.

Numerical parameters that have been used for the simulation are given in Table 3. Diffusivities  $D$  have been deduced from experimental values of single gas permeation.

## 4. Results

### 4.1. Transport

#### 4.1.1. Pd membrane

First, the thickness of the Pd membrane was estimated to be  $4.8 \mu\text{m}$  from the mass gain of the substrate

Table 4  
Single gas permeation data for MFI and Pd membranes

Membrane	Nitrogen ( $\mu\text{mol}/\text{Pa s m}^2$ )	Isobutane ( $\mu\text{mol}/\text{Pa s m}^2$ )	Hydrogen ( $\mu\text{mol}/\text{Pa s m}^2$ )
MFI	$2 \times 10^{-1}$	$10^{-2}$	$5 \times 10^{-1}$
Pd	$5 \times 10^{-2}$	$5 \times 10^{-2}$	3

assuming a continuous layer deposition. Accordingly, there was undoubtedly enough Pd to form a separative layer.

Table 4 reports permeation results. As dense Pd membranes are only permeable to hydrogen, the permeance of isobutane and nitrogen through the membrane is an indication that the separative layer contains defects or that gas leaking occurs at or in the graphite seals. However, tests with an impermeable metallic tube showed the seals were gas-tight under the present conditions.

#### 4.1.2. Zeolite membrane

Single gas permeation results are reported in Table 4 that shows MFI permeances are different from those obtained with the Pd membrane. The hydrogen/isobutane separation experiments were performed under conditions (temperature, feed flow rates, sweep) similar to those used during catalytic tests. Fig. 2 shows the separation factor  $S_f(\text{H}_2/i\text{C}_4)$  is highly dependent on both temperature and sweep flow rate. At room temperature the separation factor is close to 1 and increases up to ca. 10 at high temperature (reaction conditions).

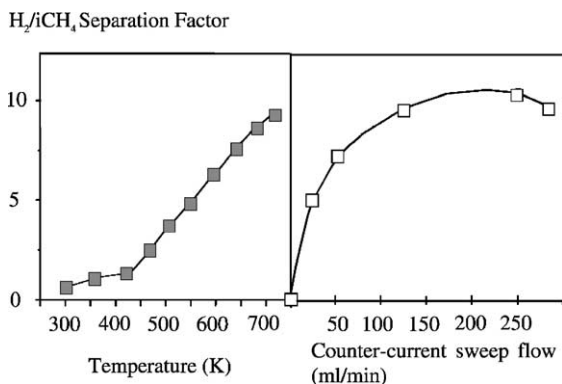


Fig. 2.  $\text{H}_2/i\text{C}_4$  separation factor  $S_f$  as a function of temperature (left) and countercurrent sweep flow rate (right).

## 4.2. CMR performance

### 4.2.1. Pd membrane reactor

Fig. 3 shows the results ( $i\text{C}_4\text{H}_{10}$  conversion and  $i\text{C}_4\text{H}_8$  yield) as a function of the sweep flow-rate. In the absence of sweep, the reactor works as a conventional one (no permeation through the membrane) and the butane conversion (14%) corresponds to that predicted by the thermodynamic equilibrium. This means that the catalyst is active enough to reach this value and that it does not suffer from deactivation during the test. These data will serve as a reference to be compared with the CMR performance.

When using a sweep, the isobutane conversion increases (Fig. 3) up to ca. 40% for a sweep flow rate of 175 ml/min (3.5 times the feed flow). This increase in conversion does however come at the cost of a slightly lower selectivity that decreases from 100 to 90%.

### 4.2.2. Zeolite membrane reactor

Most of the data have been already reported [9] and Fig. 4 shows the effect of the sweep on the isobutane conversion. The selectivity towards isobutene is also negatively affected by the sweep and varies in a similar way and range. For the highest sweep flow rate, selectivities are: isobutene 90%, *n*-butane 5%, *n*-butene 3%, C3–C1 products 2%.

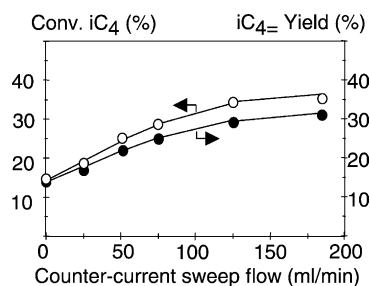


Fig. 3. Isobutane conversion and isobutene yield in the Pd membrane reactor feed flow rate: 50 ml/min, feed composition:  $\text{H}_2/i\text{C}_4/\text{N}_2 = 20/20/60$ .

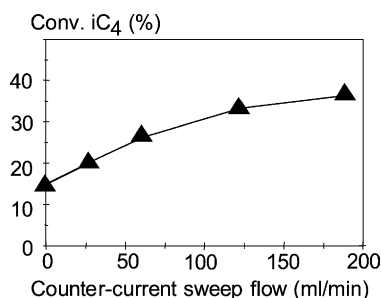


Fig. 4. Isobutane conversion yield in the MFI membrane reactor feed flow rate: 50 ml/min, feed composition:  $H_2/iC_4/N_2 = 20/20/60$ .

## 5. Discussion

### 5.1. Transport properties

#### 5.1.1. Pd membrane

When compared to data from the literature, the present Pd membrane does not show a very high performance, due to the presence of some defects. The fact that nitrogen and isobutene exhibit the very same permeances (Table 3) suggests these defects are macroporous and likely correspond to pores of the support that are not covered by Pd.

However, the  $H_2/N_2$  permselectivity (60) is clearly higher than that based on Knudsen transport (3.7). This shows the  $H_2$  permeance mainly occurs through metallic palladium.

As hydrogen and isobutane transports proceed essentially through independent pathways, the performance of the Pd membrane in  $H_2/iC_4H_{10}$  separation during CMR operation can be estimated on the basis of the calculated permselectivity (here, 60).

#### 5.1.2. MFI membrane

In this case, species ( $H_2$ ,  $N_2$ ,  $iC_4$ ) permeate through the same porous network, essentially that of the MFI material (defects contribution is limited [13]). Adsorption phenomena in the zeolite structure will rule the selectivity of the transport. At low temperature  $iC_4H_{10}$  is strongly adsorbed in the MFI pores and blocks permeation of other species. However, owing to the very small diffusivity of  $iC_4$ , its transfer through the membrane is low and close to the limited amount of  $H_2$  that may permeate, essentially through defects. Therefore, at room temperature, the  $H_2/iC_4H_{10}$  separation factor,

$S$ , is low (Fig. 1). At higher temperature,  $iC_4$  adsorption and occupancy decrease, leading to an increase of both  $H_2$  permeation and separation factor.

Fig. 2 also shows how this separation factor  $S_f$  varies with the sweep flow rate. There is a large increase of  $S_f$  in the 0–100 ml/min sweep range, then  $S$  goes through a maximum, close to 10, as high sweeps extract also  $iC_4$  in non-negligible amounts.

#### 5.1.3. Comparison of the two membranes

When compared to the MFI membrane under CMR operation conditions ( $T$ , feed, sweep), the Pd membrane shows a better performance for the  $H_2$  permeance (ca. six times higher).

As far as the  $H_2/iC_4H_{10}$  separation factor is concerned, the quantitative comparison is not so easy, as no direct measurement has been performed with the Pd membrane. However, it has been observed that most (up to 90%) of the hydrogen (coming from the feed or produced by the reaction) is extracted by the Pd membrane during CMR operation. This observation, combined with the  $H_2/iC_4H_{10}$  permselectivity of 60 deduced from single gas measurements, suggests the separation efficiency of the Pd membrane is certainly better than that of the MFI membrane under CMR operation.

### 5.2. Comparison of CMRs performances

Figs. 3 and 4 show a very similar behavior of the two MFI and Pd CMRs when increasing the countercurrent sweep flow rate.

If it is logical that the two systems give the same conversion at zero sweep (conventional reactor), it is surprising that under high sweep the Pd CMR does not draw any benefit from the better transport performances ( $H_2$  permeance and selectivity) of the Pd membrane.

In a previous publication [9], we reported on the effect of sweeping mode on the performance of the MFI CMR for the same reaction. Let us recall that, if, in the co-current sweep mode, the CMR performance was clearly controlled by the membrane, this was no more the case in the counter current sweep mode. In fact, owing to the very high driving force for hydrogen permeation that exists, in the counter current mode, at the outlet of the reactor, the catalyst was not able to establish equilibrium at the exit of the catalyst bed [9].

This interpretation is confirmed by the results shown here. As a matter of fact, the Pd membrane, with higher permeation and separation abilities, will not change the situation, as the CMR is limited by the efficiency of the (same) catalyst. Therefore, the two MFI and Pd CMRs showed similar performances.

One can speculate how to increase the catalyst performance to overcome this situation.

If the fixed-bed Pt-based catalyst is considered here as a “black-box” producing hydrogen, in competition with the membrane extracting hydrogen, it has been previously reported that this catalyst did not suffer, under similar conditions, of diffusive limitations [16]. The catalyst works therefore under chemical regime.

This catalyst has been selected after a screening of different state-of-the-art active phases in dehydrogenation reactions [16] and showed excellent activity and stability under the present conditions. It has been patented [17].

Conventional ways to improve the catalyst performance, like temperature or contact time increases, would have only limited effects. As a matter of fact, a simple calculation shows that the hydrogen production rate, at the catalyst, is much lower than the permeation rate through the membrane, at the outlet of the CMR. This extends to a factor of 30 for the MFI membrane and to a factor of 80 for the Pd membrane. Moreover, a temperature increase may deactivate the catalyst and change the selectivity. A contact time increase could result in diffusion limitations in the active phase. Furthermore, temperature and contact time increases could even improve the membrane performance, increasing again this rate gap, which is not the targeted effect.

As far as catalytic selectivity is concerned, both systems give, when increasing sweep flow, the same and limited decrease of isobutene selectivity (from 100 to 90%). This is what can be expected in the case of isobutane dehydrogenation on a Pt-zeolite-based catalyst. As a matter of fact, in this reaction, the main side reaction, isomerization (leading to the linear butane and butenes formation), goes through a dehydrogenation step of  $iC_4H_{10}$ . Therefore, the higher the sweep, the higher the isobutane dehydrogenation and, the lower the isobutene selectivity.

The fact that the two Pd and MFI CMRs give the same selectivity results also suggests that the membrane has little effect on the catalysis itself.

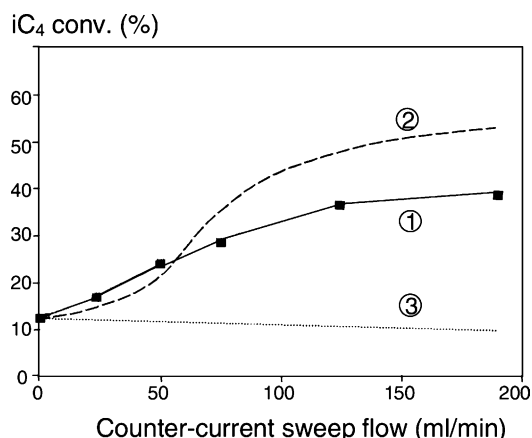


Fig. 5. Pd CMR. Comparison of experimental data (curve 1) and modeling results (curve 2). Curve 3 performance of a conventional reactor at equilibrium.

The modeling approach also shed some light on the comparison of the two CMRs. Fig. 5 (Pd CMR) and Fig. 6 (MFI CMR) compare the experimental conversions with those deduced from the modeling.

The thermodynamic equilibrium conversion in a conventional reactor is also given under similar conditions, that slightly changes with the sweep flow rate in the CMRs. As a matter of fact, owing to the pressure drop in the set-up, an increase of the sweep flow produces a pressure rise in the sweep side. To keep the transmembrane differential pressure to zero, there is a

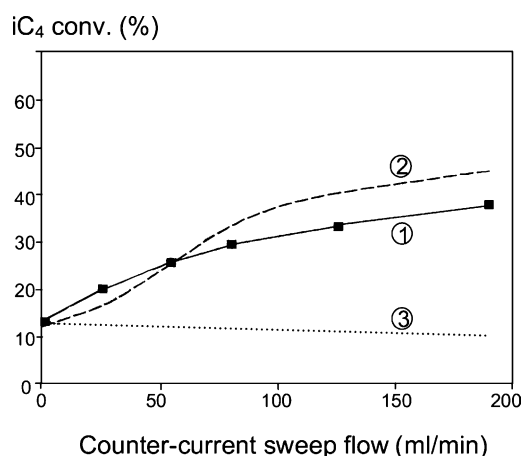


Fig. 6. MFI CMR. Comparison of experimental data (curve 1) and modeling results (curve 2). Curve 3 performance of a conventional reactor at equilibrium.

parallel pressure increase on the catalyst side. Figs. 5 and 6 show that both CMRs perform better than the conventional system.

As the model makes use of a kinetic law that has been obtained in a conventional microreactor, it predicts a performance that would have been observed only if the catalyst was not limiting. The conversion given by the model corresponds to a situation where the catalyst would be efficient enough to take into account the high hydrogen extraction and re-establish the equilibrium under conditions prevailing at the exit of the catalyst bed.

The better the membrane separative performance, the larger the gap observed between experiments and modeling. This gap can be estimated using the factor  $\eta$ , as introduced in the modeling (Eq. (3)), to account for the catalyst efficiency in the CMR. These  $\eta$  values are obtained by adjusting the model response to the experimental data. For the MFI CMR,  $\eta$  is 0.6 and only 0.4 for the Pd CMR.

## 6. Conclusion

As CMRs are made of a membrane and a catalyst, each of these two materials may control the whole performance of the reactor. In the present study of an extractor-type CMR, it has been shown that, to completely draw benefit from their combination, there was a need of developing very active catalysts, able to follow the high extraction ability of the membrane.

This observation is consistent with those already reported [1] and may be extended to other types of CMRs [9]. As a matter of fact, in a CMR, the catalyst is often placed in a reactive medium different from that existing in conventional reactors, for which catalysts have been generally designed [18].

The need of an adapted catalyst may be a general feature of CMRs, which perhaps received less attention than that dedicated to membranes.

## Appendix A. Model development

In catalyst bed,  $0 < z < L$  the mass balance on each component is

$$\frac{dF_i^{(1)}}{dz} = v_i \eta \rho \pi (R_1^2 - R_0^2) r - 2\pi R_1 N_i^m |_{r=R_1^+} \quad (\text{A.1})$$

where  $\rho$  is the catalyst apparent density defined as the mass of catalyst per internal compartment unit volume and  $v_i$  the algebraic stoichiometric coefficient of component  $i$ ,  $\eta$  the effectiveness factor introduced to take into account the limiting effects on catalyst activity in comparison with the one measured in the differential microreactor and  $r$  the kinetic rate.  $N_i^m$  is the molar flux of mixture component  $i$  through the membrane.

In the shell side, the differential equation describing mass balance in the axial direction is

$$\frac{dF_i^{(2)}}{dz} = (-1)^n 2\pi R_3 N_i^s |_{r=R_3^-} \quad (\text{A.2})$$

with  $n = 0$  for co-current and  $n = 1$  for counter current.  $N_i^s$  is the molar flux of mixture components through the support.

In the membrane the conservation of the mass balance is

$$\frac{1}{r} \frac{\partial}{\partial r} (r N_i^m) = 0 \quad (\text{A.3})$$

with

$$N_i^m = -\frac{D_i^m \varepsilon_m}{RT \tau_m} \frac{\partial P_i^m}{\partial r} \quad (\text{A.4})$$

In the support a similar expression is derived

$$\frac{1}{r} \frac{\partial}{\partial r} (r N_i^s) = 0 \quad (\text{A.5})$$

and

$$N_i^s = -\frac{D_i^s \varepsilon_s}{RT \tau_s} \frac{\partial P_i^s}{\partial r} \quad (\text{A.6})$$

Expressions (A.3) and (A.5) are solved analytically taking into account the following boundary conditions:

$$\text{at } r = R_1 \quad P_i^m |_{r=R_1^+} = P_i^{(1)} = \frac{F_i^{(1)}}{F_T^{(1)}} P \quad (\text{A.7})$$

$$\text{at } r = R_2 \quad P_i^m |_{r=R_2^-} = P_i^s |_{r=R_2^+} \quad (\text{A.8})$$

$$\text{at } r = R_3 \quad P_i^s |_{r=R_3^-} = P_i^{(2)} = \frac{F_i^{(2)}}{F_T^{(2)}} P \quad (\text{A.9})$$

and the continuity of flux at the interface membrane/support ( $N_i^m = N_i^s$ ) to obtain the following

equation of the molar flux through the membrane:

$$N_i^m|_{r=R_1^+} = -\frac{1}{R_1} \frac{D_i^m \varepsilon_m}{\tau_m} \frac{1}{\ln(R_2/R_1) + (D_i^m \varepsilon_m / D_i^s \varepsilon_s) \frac{P}{RT} \times (\tau_s / \tau_m) \ln(R_3/R_2)} \times \left( \frac{F_i^{(2)}}{F_T^{(2)}} - \frac{F_i^{(1)}}{F_T^{(1)}} \right) \quad (\text{A.10})$$

Substituting Eq. (A.10) in Eq. (A.1) the mass balance in the tube can be written as

$$\frac{dF_i^{(1)}}{dz} = v_i \eta \rho \pi (R_1^2 - R_0^2) r + 2\pi \frac{P}{RT} \frac{D_i^m \varepsilon_m}{\tau_m} \frac{1}{\ln(R_2/R_1) + (D_i^m \varepsilon_m / D_i^s \varepsilon_s) \times (\tau_s / \tau_m) \ln(R_3/R_2)} \times \left( \frac{F_i^{(2)}}{F_T^{(2)}} - \frac{F_i^{(1)}}{F_T^{(1)}} \right) \quad (\text{A.1}')$$

Using at steady-state the conservation of the flux at the interface membrane/support in the radial direction

$$N_i^s|_{r=R_3^-} = \frac{R_1}{R_3} N_i^m|_{r=R_1^+} \quad (\text{A.11})$$

Eq. (A.2) becomes

$$\frac{dF_i^{(2)}}{dz} = (-1)^{n+1} 2\pi \frac{P}{RT} \frac{D_i^m \varepsilon_m}{\tau_m} \frac{1}{\ln(R_2/R_1) + (D_i^m \varepsilon_m / D_i^s \varepsilon_s) \times (\tau_s / \tau_m) \ln(R_3/R_2)} \times \left( \frac{F_i^{(2)}}{F_T^{(2)}} - \frac{F_i^{(1)}}{F_T^{(1)}} \right) \quad (\text{A.12})$$

Due to chemical reaction and back permeation, the total molar rate vary along the membrane length. The total molar flux in tube  $F_T^{(1)}$  is obtained from overall mass balance by adding together Eq. (A.1) written for each component of the gaseous mixture:

$$\frac{dF_T^{(1)}}{dz} = -2\pi R_1 \sum_i N_i^m|_{r=R_1^+} + \eta \rho \pi (R_1^2 - R_0^2) r \Delta v \quad (\text{A.13})$$

where  $\Delta v = \sum_i v_i$ .

The total molar flux at the interface membrane tube is defined by

$$\sum_i N_i^m|_{r=R_1^+} = -\frac{1}{RT} \sum_i \frac{D_i^m \varepsilon_m}{\tau_m} \frac{\partial P_i^m}{\partial r} \Big|_{r=R_1^+} \quad (\text{A.14})$$

We assume the total pressure to be constant, therefore the variation of the inert partial pressure through the membrane is

$$\frac{\partial P_I^m}{\partial r} = -\sum_{j \neq I} \frac{\partial P_j^m}{\partial r} \quad (\text{A.15})$$

where “I” symbolizes the inert component or sweep gas. Substituting Eq. (A.15) in Eq. (A.14) combined with Eqs. (A.4) and (A.10), the radial total molar flux can be determined by the expression

$$\sum_i N_i^m|_{r=R_1^+} = \frac{1}{R_1} \frac{P}{RT} \sum_{j \neq I} \frac{(D_I^m - D_j^m) \varepsilon_m}{\tau_m} \frac{1}{\ln(R_2/R_1) + (D_i^m \varepsilon_m / D_i^s \varepsilon_s) \times (\tau_s / \tau_m) \ln(R_3/R_2)} \times \left( \frac{F_i^{(2)}}{F_T^{(2)}} - \frac{F_i^{(1)}}{F_T^{(1)}} \right) \quad (\text{A.16})$$

Substituting Eq. (A.16) in Eq. (A.13), the overall mass balance is

$$\frac{dF_T^{(1)}}{dz} = -2\pi \frac{P}{RT} \sum_{j \neq I} \frac{(D_I^m - D_j^m) \varepsilon_m}{\tau_m} \frac{1}{\ln(R_2/R_1) + (D_i^m \varepsilon_m / D_i^s \varepsilon_s) \times (\tau_s / \tau_m) \ln(R_3/R_2)} \times \left( \frac{F_i^{(2)}}{F_T^{(2)}} - \frac{F_i^{(1)}}{F_T^{(1)}} \right) + \eta \rho \pi (R_1^2 - R_0^2) r \Delta v \quad (\text{A.17})$$

In the shell side the material balances for all the components is

$$\frac{dF_T^{(2)}}{dz} = (-1)^n 2\pi R_3 \sum_i N_i^s|_{r=R_3^-} \quad (\text{A.18})$$

By substituting Eqs. (A.11) and (A.16) in Eq. (A.18), the overall mass balance becomes

$$\begin{aligned} \frac{dF_T^{(2)}}{dz} &= (-1)^n 2\pi \frac{P}{RT} \sum_{j \neq I} \frac{(D_I^m - D_j^m) \varepsilon_m}{\tau_m} \\ &\times \frac{1}{\ln(R_2/R_1) + (D_I^m \varepsilon_m / D_I^s \varepsilon_s)} \\ &\quad \times (\tau_s / \tau_m) \ln(R_3/R_2) \\ &\times \left( \frac{F_i^{(2)}}{F_T^{(2)}} - \frac{F_i^{(1)}}{F_T^{(1)}} \right) \end{aligned} \quad (\text{A.19})$$

## References

- [1] S. Mota, S. Miachon, J.-C. Volta, J.-A. Dalmon, *Catal. Today* 67 (2001) 169.
- [2] H.P. Hsieh, *Inorganic Membranes for Separation and Reaction*, Elsevier, Amsterdam, 1996, p. 299.
- [3] E. Piera, C. Tellez, J. Coronas, M. Menendez, J. Santamara, *Catal. Today* 67 (2001) 127.
- [4] T. Matsuda, I. Koike, N. Kubo, E. Kikuchi, *Appl. Catal. A* 96 (1993) 3.
- [5] B.A. Raich, H.C. Foley, *Appl. Catal. A* 129 (1995) 167.
- [6] J. Shu, B.P.A. Grandjean, S. Kaliaguine, P. Ciavarella, A. Giroir-Fendler, J.-A. Dalmon, *Can. J. Chem. Eng.* 75 (1997) 712.
- [7] T. Ionnides, G.R. Gavalas, *J. Membr. Sci.* 77 (1993) 207.
- [8] Y. Zhu, R.G. Minet, T.T. Tsotsis, *Catal. Lett.* 18 (1993) 48.
- [9] P. Ciavarella, D. Casanave, H. Moueddeb, S. Miachon, K. Fiaty, J.-A. Dalmon, *Catal. Today* 67 (2001) 177.
- [10] U. Illgen, R. Schäfer, M. Noack, P. Kölsch, A. Kühnle, J. Caro, *Catal. Commun.* 2 (2001) 339.
- [11] P. Mériaudeau, A. Thangaraj, C. Naccache, *Stud. Surf. Sci. Catal. B* 101 (1996) 1313.
- [12] J. Keuler, L. Lorenzen, S. Miachon, *Sep. Sci. Technol.* 37 (2) (2002) 379.
- [13] A. Giroir-Fendler, J. Peureux, H. Mozzanega, J.-A. Dalmon, *Stud. Surf. Sci. Catal. A* 101 (1996) 127.
- [14] D. Casanave, P. Ciavarella, K. Fiaty, J.-A. Dalmon, *Chem. Eng. Sci.* 54 (1999) 2807.
- [15] D. Casanave, K. Fiaty, J.-A. Dalmon, M. Forissier, *Stud. Surf. Sci. Catal.* 122 (1999) 367.
- [16] D. Casanave, Ph.D. Thesis, Lyon University, 1996.
- [17] P. Mériaudeau, P. Nascimento, G. Sapaly, C. Naccache, European Patent EP98400371.5-2104.
- [18] J.-A. Dalmon, *Handbook of Heterogeneous Catalysis*, in: Ertl, Knözinger, Weitkamp (Eds.), VCH, Weinheim, 1997, Chapter 9.3, p. 1387.